

## Research Article

# Detection of Chemical Weapon Agents Using Spectroscopic Probes: A Computational Study

Letícia S. Braga,<sup>1</sup> Érika F. Silva,<sup>1</sup> Daiana T. Mancini,<sup>1</sup> Eduardo P. da Rocha,<sup>2</sup>  
Elaine F. F. da Cunha,<sup>1</sup> and Teodorico C. Ramalho <sup>1,3</sup>

<sup>1</sup>Department of Chemistry, Federal University of Lavras, University Campus, Lavras 37200-000, MG, Brazil

<sup>2</sup>Institute Federal of Science, Education and Technology of Southwest MG, Campus Rio Pomba, Rio Pomba 36180000, MG, Brazil

<sup>3</sup>Department of Chemistry, Faculty of Science, University of Hradec Kralove, Hradec Kralove, Czech Republic

Correspondence should be addressed to Teodorico C. Ramalho; teo@dqj.ufla.br

Received 4 October 2019; Revised 5 March 2020; Accepted 19 March 2020; Published 21 April 2020

Academic Editor: João Paulo Leal

Copyright © 2020 Letícia S. Braga et al. This is an open access article distributed under the Creative Commons Attribution License, which permits unrestricted use, distribution, and reproduction in any medium, provided the original work is properly cited.

Organophosphorus compounds are organic compounds widely employed in agriculture as well as in chemical weapons. The use in agriculture is due to their insecticidal properties. However, in chemical warfare, the use of organophosphorus is associated with acetylcholinesterase inhibition, which promotes the cholinergic syndromes. In this line, the fast detection of this class of compound is crucial for the determination of environmental exposure. This improved detection will naturally allow for more prompt courses of treatment depending on the contaminant findings. In this perspective, the dipyrinone oxime (**1**) was employed for the detection of organophosphorus compounds that are employed as nerve agents, such as cyclosarin, sarin, soman, diethyl chlorophosphate, diisopropylfluorophosphate, 2-(dimethylamino)ethyl N,N-dimethylphosphoramidofluoridate, O-ethyl-S-[2-(diethylamino)ethyl]methylphosphonothioate, O-ethyl-S-[2(diisopropylamino)ethyl] methylphosphonothioate, and O,O-diethyl-S-[2-(diethylamino)ethyl] phosphorothioate, through fluorescent emission. The thermodynamics and kinetic parameters as well as spectroscopic properties of the complexes formed for **1** and all organophosphorus compounds previously cited were investigated by means of theoretical calculations. From our findings, only the diethyl chlorophosphate, 2-(dimethylamino)ethyl N,N-dimethylphosphoramidofluoridate, and O,O-diethyl-S-[2-(diethylamino)ethyl] phosphorothioate emitted fluorescence in the hexane, toluene, chloroform, dichloromethane, methanol, acetonitrile, water, and dimethyl sulfoxide solvents. The study of the absorption wavelength with the most polar solvent showed higher values compared to apolar solvents. In the same solvent, for instance, soman in hexane showed the lowest absorption wavelength value, 324.5 nm, and DCP the highest value, 330.8 nm. This behavior was observed in other tested solvents. The thermodynamic parameters indicate negative Gibbs free energy ( $\Delta G$ ) values for the O-ethyl-S-[2(diisopropylamino)ethyl] methylphosphonothioate with **1** reaction. On the other hand, the sarin and cyclosarin revealed the lowest Gibbs free energy ( $\Delta G^\ddagger$ ) values, being kinetically favorable and presenting more reactivity.

## 1. Introduction

Organophosphorus (OP) compounds are organic compounds that have, at least, one carbon-phosphorus chemical bond. The first OP compounds were prepared in the Middle Ages, but in the XIX century, their study became more intense by Michaelis [1–3]. In 1930, toxic and insecticidal properties of these compounds were reported [4]. Since then, there has been growing interest in the study of this class of compounds due to their possible application as agrochemicals and chemical weapons [5, 6]. The high toxicity of the OP

compounds is associated with high affinity for the acetylcholinesterase enzyme [7, 8]. Actually, it is well known that OP compounds can form a stable chemical bond with the serine amino acid residue present in the active site of the acetylcholinesterase enzyme (AChE) [8, 9]. Among the main nerve agents, it is possible to highlight the compounds cyclosarin, sarin, soman, DCP (diethyl chlorophosphate), DFP (diisopropylfluorophosphate), GV (2-(dimethylamino)ethyl N,N-dimethylphosphoramidofluoridate), VM (O-ethyl-S-[2-(diethylamino)ethyl]methylphosphonothioate), VX (O-ethyl-S-[2(diisopropylamino)ethyl]

methylphosphonothioate), and VG (O,O-diethyl-S-[2-(diethylamino)ethyl] phosphorothioate) (Figure 1).

It should be kept in mind, however, that the reactivation reaction can occur by spontaneous hydrolysis, which is a very slow process, or by using oximes, which are considered AChE reactivators [10, 11].

To date, the use of oximes is the most efficient approach aiming at AChE reactivation [12, 13]. The AChE inhibition process can be illustrated in Scheme 1 [14].

Although the use of OP compounds as chemical weapons has called much attention and generated wide discussion in the international community [15, 16], it is important to keep in mind that the abusive use of OP compounds, as agrochemicals, is dangerous [16]. Currently, the use and misuse of OP compounds in agriculture are responsible for the majority of poisonings in Brazil [4, 16].

In view of this scenario, the detection and quantification of OP compounds in the environment are crucial [2]. In 2013, Walton et al. suggested the use of fluorescent techniques to detect OP compounds [17]. In fact, when OP compounds bind to a fluorescent probe, such as dipyrinone oxime (2-ethyl-7-[(Z)-(hydroxyimino)methyl]-1-methyl-3H-dipyrrolo[1,2-c:2',1'-f]pyrimidine-3,5-dione), the color changes from red to yellow (Scheme 2) [17].

Despite several efforts to apply fluorescent probes for OP detection, there is still a dearth of systematic understanding of the thermodynamics of guest-responsive hybrid frameworks. In this perspective, the theoretical work could be an ally in the rationalization of thermodynamics and spectroscopic properties of these materials [18]. Furthermore, theoretical approaches provide an economically viable route for applications, as these methods can also open a new avenue to study the structural modifications, which could optimize the detection of OP compounds [19].

Thus, aiming at combining efficiency and selectivity in the OP compound detection process, this paper is devoted to the theoretical study of spectroscopic properties of nerve agents as fluorescent probes.

## 2. Methodology

The oxime-organophosphorus complex calculations were carried out in the ground and the excited states using the DFT and TD-DFT levels [20, 21], respectively. Six different functionals were tested (B3LYP, CAM-B3LYP, B3PW91, MPW1PW91, PBEPBE, and  $\omega$ B97XD) [22, 23]. The functional that best approached the wave function theoretical result with respect to the experimental result was selected for performing the calculations together with the DGTZVP basis set. For the potential energy surface, the surface response was employed that was developed by selecting two  $\alpha_1$  (C26, C28, C29, and C31) and  $\alpha_2$  (C29, C31, C32, and C33) dihedral angles according to Figure 2. The energy for the ground and excited states was calculated, and a potential energy surface scan of dihedral angles  $\alpha_1$  and  $\alpha_2$  from  $-180$  to  $180^\circ$  was performed, according to Table 1. The effect of the methanol solvent on the surface response was carried out by employing IEFPCM [24] for each point of the surface.

All compounds involved in the reaction described in Scheme 2 were optimized and the frequency was calculated at the DFT/B3LYP/DGTZVP level. The transition state was evaluated using Spartan quantum software [25]. The imaginary frequency for all transition states was determined at the DFT/B3LYP/DGTZVP level [26, 27]. The relaxation of the solvent was investigated using the Tamm-Dancoff approximation (TDA) [28–30] for the nine organophosphorus compounds (cyclosarin, DCP, DFP, GV, sarin, soman, VG, VM, and VX) complexed with the dipyrinone oxime (**1**), taking into account the effect of the solvents (such as hexane, acetonitrile, methanol, toluene, chloroform, dichloromethane, dimethyl sulfoxide, and water). The TDA is a computationally simple method for molecular excited states, which can be used for predicting vibrationally resolved absorption and emission spectra of diverse molecules [28–30]. These calculations were performed in conjugation with the TD-DFT method for the solvent relaxation and spectroscopic property calculation investigation for each oxime/organophosphorus compound. All spectroscopic calculations were carried out in Orca quantum chemistry [31].

## 3. Results and Discussion

*3.1. Selection of the DFT Functional for Spectroscopic Calculations.* The spectroscopic properties of the complexes formed by **1** and the organophosphorus compounds studied (Figure 2) were evaluated by both DFT and TD-DFT methods. At the first moment, the selection of the best DFT functional was performed by error calculation in the absorption wavelength value for the oxime (**1**)/DFP complex. This complex showed an absorption wavelength at 400 nm.

TD-DFT/DGTZVP was employed in conjugation with the DFT functionals B3LYP, CAM-B3LYP, B3PW91, MPW1PW91, PBE, and  $\omega$ B97XD with the IEFPCM model for methanol, which was used in the experimental part. These functionals were tested for behold different families: meta-GGA, hybrid functional, and long-range hybrid functional. The compound geometric properties showed similarity in the DFT and TD-DFT methods, which allowed us to apply the same geometries in the ground and excited states. The bond lengths are similar for geometries generated by both methods, for instance, the P atom bounded with the three oxygen atoms in VG, DFP, and DCP and the P atom bonded to N, C, or S atoms in VG, VM, sarin, and soman. The distances between P and these atoms are reported in Supplementary Material, Table S3. In the same cases, the distance between P=O was around 1.46 Å, and the other O atoms showed values between 1.58 and 1.71 Å. The distance between P and F or Cl atoms was 1.68 Å, and the distance between P and S atom was 2.70 and 1.61 Å. After the reaction with oxime, all distances showed the same values, but the atoms bound with P atom were changed. In the same cases, the P atom linked with four O atoms with 1.80 at 1.64 Å.

From our findings, the best functional for the spectroscopic properties investigated was the B3LYP hybrid functional. The error for the B3LYP functional was 7.1 nm, while for B3PW91 it was  $-9.31$  nm and for MPW1PW91 it

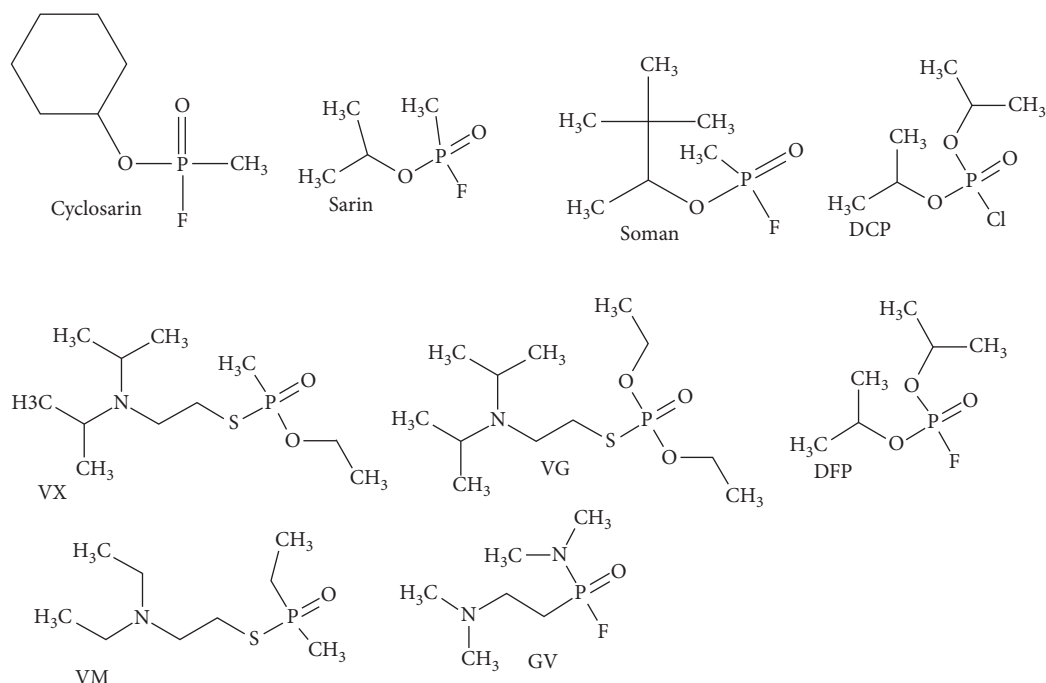
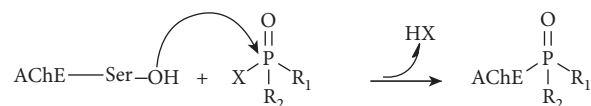
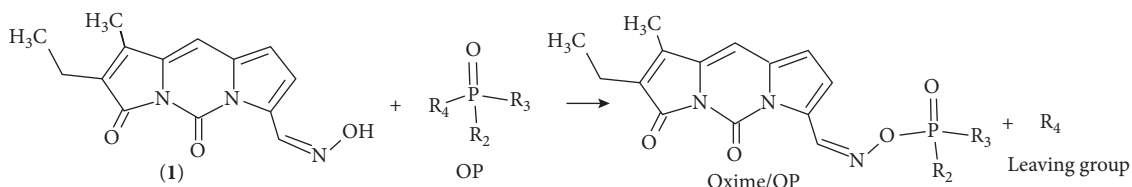


FIGURE 1: Chemical structure of organophosphorates employed with fluorescent probes.



SCHEME 1: Inhibition scheme of acetylcholinesterase enzyme by organophosphate, where R<sub>1</sub> is the alkyl group, O alkyl or amide; R<sub>2</sub> the O alkyl group or amide; and X the leaving group. The reaction pathway followed by acetylcholinesterase consists primarily in the activation of a water molecule, followed by the attack to the central phosphorus, leading to a change of configuration.



SCHEME 2: Colorimetric reaction between dipyrinone oxime with organophosphates generating complex fluorescent oxime/organophosphates, where R<sub>4</sub> is the leaving group. R<sub>2</sub> and R<sub>3</sub> were other specific substituents in the compounds.

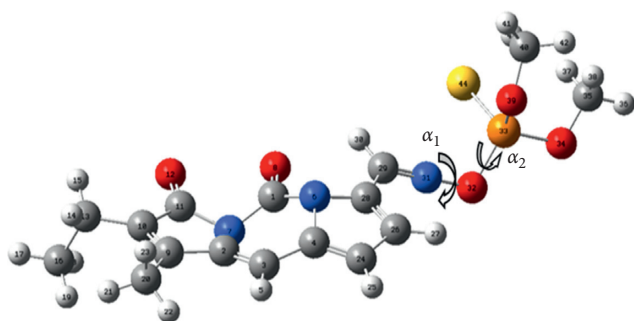


FIGURE 2: The dihedral angles  $\alpha_1$  and  $\alpha_2$  employed for building the surface response model in the oxime-organophosphorus complex.

TABLE 1: Wavelength values for each functional studied and the respective error value.

DFT functional**	Wavelength (nm)	Error (nm)
B3LYP	407.1	7.1
CAM-B3LYP	347.13	-52.87
B3PW91	390.69	-9.31
MPW1PW91	386.78	-13.22
PBEPBE	478.82	78.82
$\omega$ B97XD	345.25	-54.75
Experimental	400*	—

\*Experimental value according to Walton et al. [17]. \*\*B3LYP (Becke, 3-parameter, Lee-Yang-Parr); MPW1PW91 (hybrid Hartree-Fock density functional); PBEPBE (Perdew-Burke-Ernzerhof).

was  $-13.22$  nm (Table 1). On the other hand, the CAM-B3LYP and  $\omega$ B97XD long-range hybrid functional [32–35] showed higher error values,  $-52.87$  nm and  $-54.75$  nm, respectively. The PBE meta-GGA functional showed an error value of  $78.82$  nm, the highest error for the spectroscopic properties (Table 1).

The ANQ geometry for the enol and keto forms was optimized at the DFT level employing the six DFT functionals cited above, the B3LYP showed results with lower deviation between  $n \rightarrow \pi^*$  and  $\pi \rightarrow \pi^*$  and a good agreement with hybrid functional and long-range hybrid functional (CAM-B3LYP and  $\omega$ B97XD) for the  $\pi$  conjugation [28, 36–38].

The B3LYP functional selected in the study was employed for the optimization in the ground state as well as in the theoretical calculations of twenty excited states for all compounds because the first 20 excited states give a good description of the electronic parameters for organophosphorus compounds [36, 39–41].

**3.2. Response Surface Analysis.** It is well known that spectroscopic properties are modulated by structural features [42–46]. Thus, to take into account the geometric effects on the nerve agents, we have used chemometric techniques, such as surface response methodology [47].

The response surface (RS) is a design of experiment (DOE) methodology employed for optimization (in this case minimization) of response [48, 49] The RS is based on the factorial design with a central point and using the quadratic equation provides for minimum response with the least number of experiments (in this case theoretically calculated) [50, 51]. The response surface was used to obtain the energy minimum in relation to the two  $\alpha_1$  and  $\alpha_2$  dihedral angles (Figure 2). The dihedral angles were modified from  $-180$  to  $180^\circ$  according to that described in Supplementary Information Tables S1 and S2. The surface response in the gas phase is presented in Figure 3, which describes the optimization obtained using the employed response surface that connected the variation of  $\alpha_1$  and  $\alpha_2$  angles (see Figure 2) with the energy variation calculated by the B3LYP/DGTZVP method. The results indicated that the variation of angles in the studied compounds modified the calculated energy. The optimization generated the contour graph, the 2D dimension plot, as well as the contours map described in the surface and put in evidence the minimum energy values for dihedral angles [52, 53]. In the gas phase, the energy minimum is associated with  $\alpha_1$  dihedral angle of  $25^\circ$  and with  $\alpha_2$  dihedral angle of  $0^\circ$ . On the other hand, Figure 4 shows the same angles for the compounds in the solvent, which also describes the optimization obtained using the response surface, which connected the variation of angles  $\alpha_1$  and  $\alpha_2$  to the variation of energy calculated by the same method mentioned above; however, the oxime/organophosphate complex is in methanol.

From the dihedral angles (Figure 3), the spectroscopic properties were obtained for all analyzed compounds. The OPs analyzed were sarin, soman, DCP, DFP, cyclosarin, GV, VX, VM, and VG. Interestingly, all complexes formed

between OP and the spectroscopic probe **I** showed the same dihedral angles for the energy minimum. Thus, the dihedral angles were fixed for all compounds for the TD-DFT/DGTZVP/B3LYP spectroscopic property calculations in the gas phase, as well as in the other eight solvents (hexane, chloroform, dichloromethane, toluene, methanol, acetonitrile, water, and DMSO).

**3.3. Thermodynamics and Kinetic Parameters for the Reaction between Oxime (I) and Nerve Agents.** The thermodynamic and kinetic parameters for the colorimetric reaction described in Scheme 2 were calculated using the DFT methodology. The **I** reacted with each OP compound forming the oxime/OP complex, having the leaving group ( $R_4$ ) according to the OP employed. The  $S_N2$  reaction mechanism was employed for this reaction [1] The enthalpy ( $\Delta H$ ), Gibbs free energy for reaction ( $\Delta G$ ), transition state Gibbs free energy ( $\Delta G^\ddagger$ ) values, and rate constants were calculated for the analysis of the spontaneity of this reaction. The thermodynamic and kinetic parameters are shown in Table 2.

Reaction **I**, employing the cyclosarin compound as substrate and fluorine as a leaving group, showed the  $\Delta H$  value of  $-2.49$  kcal/mol. This process was exothermic and the activation Gibbs free energy ( $\Delta G^\ddagger$ ) for reaching the transition state was  $15.68$  kcal/mol. It was possible to observe that reaction **II** showed higher  $\Delta G$ ,  $\Delta H$ , and  $\Delta G^\ddagger$  values than reaction **I**. The reaction **II** employed the DCP compound and the chlorine as leaving group. The  $\Delta H$  for this reaction was the highest among the endothermic reactions (see Table 2).

Now, by analyzing the other reactions having the fluorine as leaving group, it is possible to notice that reaction **III**, employing DFP as OP, showed  $1.80$  and  $6.49$  kcal/mol for  $\Delta H$  and  $\Delta G$ , respectively. Thus, this reaction is endothermic and is not spontaneous. The reactions **IV**, **V**, and **VI** were exothermic with  $\Delta H$  values of  $-0.51$ ,  $-2.50$ , and  $-2.53$  kcal/mol, respectively. Thus, having the fluorine as the leaving group, only reaction **III** was endothermic. The  $\Delta G$  values for the reactions **IV**, **V**, and **VI** were  $6.44$ ,  $2.68$ , and  $3.08$  kcal/mol, respectively. Similarly, all reactions were not spontaneous. The other four reactions exhibit the sulfur group as the leaving group. The reactions **VII** and **VIII** showed the 2-[di(propan-2-yl)amino]ethanethiolate compound as the leaving group, while the reactions **IX** exhibit the 2-(diethylamino)ethanethiolate as the leaving group. The reactions **VII** and **VIII** showed  $\Delta H$  values of  $0.37$  and  $0.28$  kcal/mol while the  $\Delta G$  values were  $0.69$  and  $0.40$  kcal/mol, respectively. Although the reaction showed positive  $\Delta H$  and  $\Delta G$  values, these systems were the most promising among the studied reactions without the sulfur group as the leaving group. The reaction **IX** showed the  $\Delta H$  value of  $0.08$  kcal/mol and the  $\Delta G$  value of  $-0.23$  kcal/mol. The reaction **IX** was endothermic and spontaneous.

Turning now to kinetic studies, the  $\Delta G^\ddagger$  values (Figure 5) were positive for all studied reactions, which is according to the transition state theory. Surprisingly, the halogen derivatives indicated the lowest  $\Delta G^\ddagger$  values, probably due to lower steric hindrance. This fact was observed in reactions

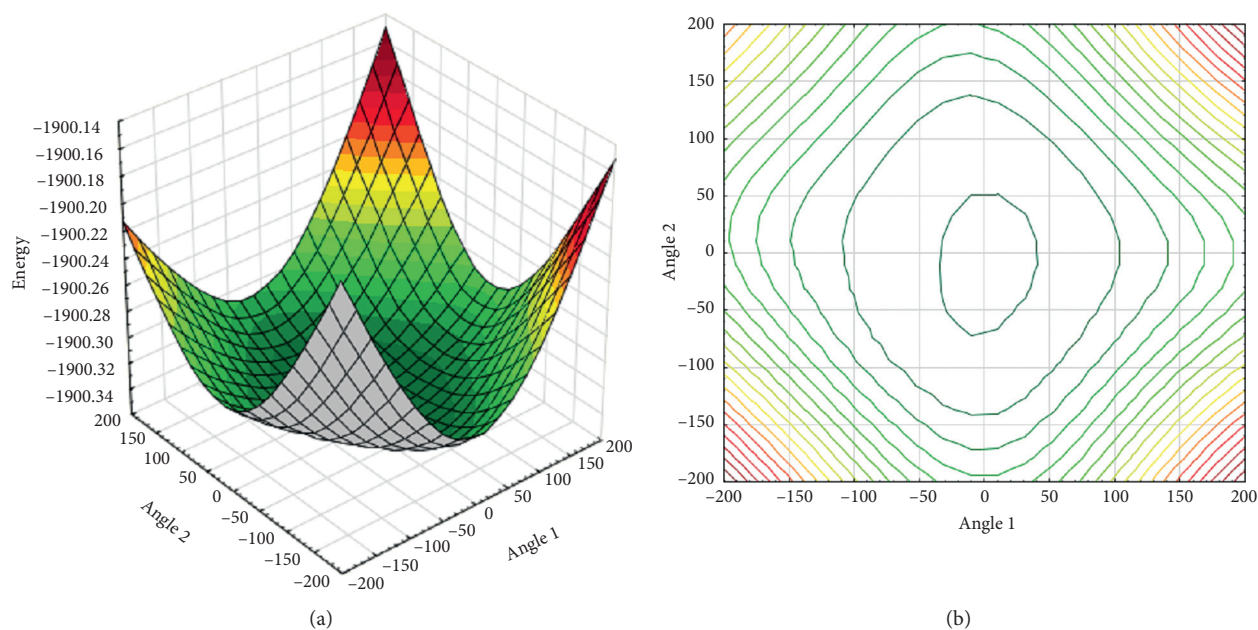


FIGURE 3: (a) Surface response of the oxime/organophosphate complex showing the energy minimum for the dihedral angles  $\alpha_1$  and  $\alpha_2$  in the gas phase. (b) The contour graph of the potential surface of the oxime/diisopropylfluorophosphate complex showing the energy minimum for the dihedral angles  $\alpha_1$  and  $\alpha_2$  in the gas phase.

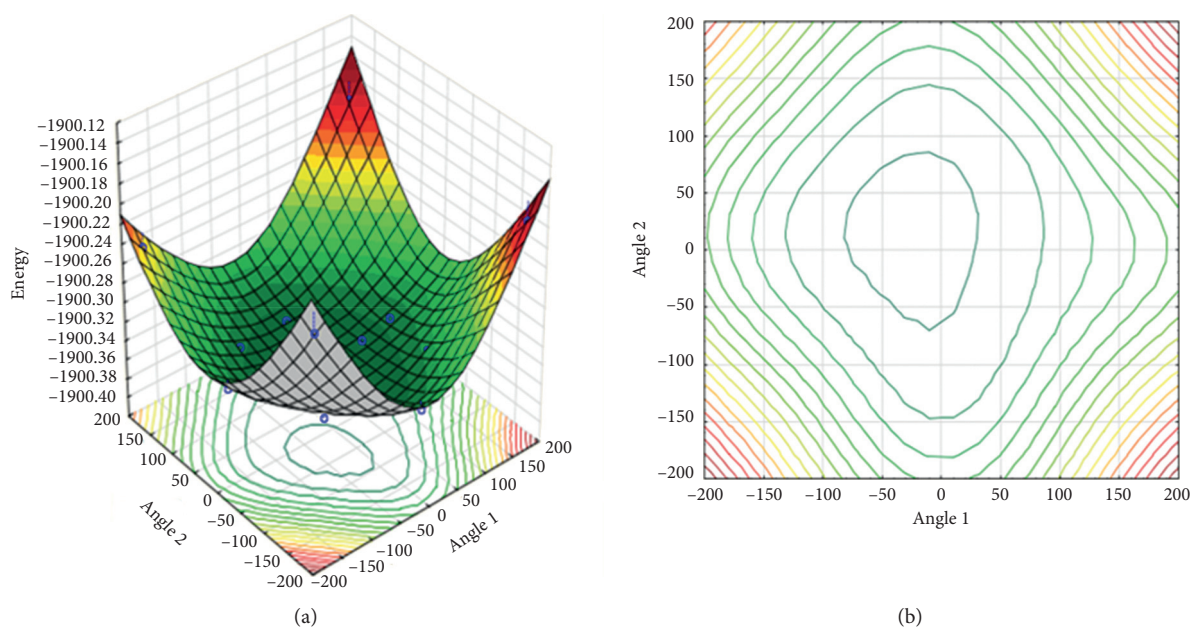


FIGURE 4: (a) Surface response of the oxime/diisopropylfluorophosphate complex showing the energy minimum for the dihedral angles  $\alpha_1$  and  $\alpha_2$  in methanol. (b) Contour graph of the potential surface of the oxime/organophosphate complex showing the energy minimum for the dihedral angles  $\alpha_1$  and  $\alpha_2$  in methanol.

VII, VIII, and IX, where there is the presence of more bulky substituents as leaving groups. In fact, it is well known that steric factors are crucial for  $S_N2$  reactions.

Furthermore, the rate constant ( $k$ ) was also calculated employing the Eyring equation [54–57] according to equation (1). The rate constant demonstrates that sarin is more reactive, while VM was less reactive among the OPs.

Therefore, the reactivity order was sarin > cyclo sarin > DFP > DCP > GV > VG > VM > VX. The chemical reactions for VX were thermodynamically favorable, which can be characterized by negative  $\Delta G$  values. The reaction with cyclosarin and sarin was the most kinetically favorable among all, revealing the lowest  $\Delta G^\ddagger$  value. It should be kept in mind that all OP compounds were kinetically, but not

TABLE 2: Thermodynamic and kinetic parameters (kcal/mol) for the colorimetric reaction between oxime and organophosphates (OP) according to Figure 3.

Reaction	OP*	Leaving group	Enthalpy ( $\Delta H$ )	Transition state Gibbs free energy ( $\Delta G^\ddagger$ )	Reaction Gibbs free energy ( $\Delta G$ )	Rate constant ( $k$ )
I	Cyclosarin	F	-2.49	15.68	3.49	$6.17E+12$
II	DCP	Cl	2.42	18.74	6.37	$6.16E+12$
III	DFP	F	1.80	16.82	6.49	$6.17E+12$
IV	GV	F	-0.51	18.01	6.44	$6.16E+12$
V	Sarin	F	-2.50	15.17	2.68	$6.18E+12$
VI	Soman	F	-2.53	18.50	3.08	$6.16E+12$
VII	VG	$S(CH_2)_2N(CH_2(CH_3)_2)_2$	0.37	25.09	0.69	$6.15E+12$
VIII	VM	$S(CH_2)_2N(CH_2(CH_3)_2)_2$	0.28	53.53	0.40	$6.08E+12$
IX	VX	$S(CH_2)_2N(CH_2CH_3)_2$	0.08	61.36	-0.23	$6.06E+12$

\*DCP (diethyl chlorophosphate), DFP (diisopropylfluorophosphate), GV (2-(dimethylamino)ethyl N,N-dimethylphosphoramidofluoridate), VM (O-ethyl-S-[2-(diethylamino)ethyl]methylphosphonothioate), VX (O-ethyl-S-[2(diisopropylamino)ethyl] methylphosphonothioate), and VG (O,O-diethyl-S-[2-(diethylamino)ethyl] phosphorothioate).

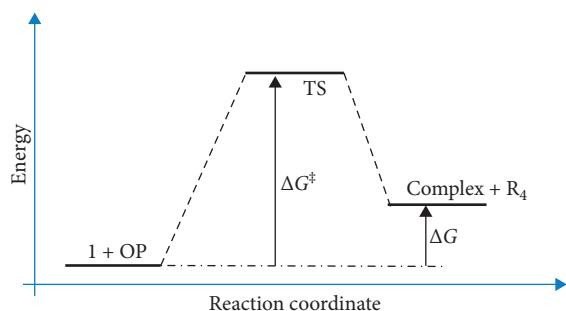


FIGURE 5: Diagram for the reaction between 1 and organophosphates as demonstrated in Figure 3. The  $\Delta G^\ddagger$  is the transition state Gibbs free energy and  $\Delta G$  is the Gibbs free energy for reaction.

thermodynamically, favorable for the colorimetric detection reaction of nerve agents (Scheme 2):

$$k = \frac{k_B T}{h} \exp\left(-\frac{\Delta G^\ddagger}{RT}\right). \quad (1)$$

3.4. *Spectroscopic Properties of the Oxime/Organophosphate Complex.* The complexes formed between the oxime derivatives and OPs are displayed in Scheme 2. The compounds formed by the reaction of nine OPs with the oxime (Table 3) also have their spectroscopic properties calculated.

The absorption wavelengths of all complexes in eight solvents are reported in Table 4. The spectroscopic parameters were calculated by using the ORCA program at the TD-DFT/DGTZVP/B3LYP level, incorporating the Tamm–Dancoff approximation for evaluating the solvent relaxation as well as the absorption and emission energy for all compounds.

The study of the absorption wavelength with the most polar solvent showed higher values compared to apolar solvents. In the same solvent, for instance, soman in hexane showed the lowest absorption wavelength value (324.5 nm), followed by DFP (325.9 nm), sarin (326.2 nm), VM (326.4 nm), VG (327.7 nm), VX (327.9 nm), cyclosarin (328 nm), GV (329.4 nm), and DCP (330.8 nm). This

behavior was observed in other tested solvents. For the same OPs, for example, GV, the absorption wavelength was according to the following order: hexane (329.4 nm), toluene (329.3 nm), chloroform (326.2 nm), dichloromethane (326.5 nm), methanol (325.7 nm), acetonitrile (325.8 nm), water (325.7 nm), and DMSO (326.4 nm). All values for the other compounds are described in Table 4. In fact, the constant dielectric ( $\delta$ ) value of the studied solvents influences the absorption wavelength. The solvent hexane ( $\delta = 80$ ), which shows the highest constant dielectric value in the studied series. Other solvent properties, such as the dipolar moment ( $\vec{\rho}$ ), can also be taken. From our findings, hexane ( $\vec{\rho} = 0D$ ) showed lowest absorption wavelength value compared to DMSO ( $\vec{\rho} = 3.96D$ ), according to Table 3. In this line, the dipolar moment can, in principle, rationalize the behavior observed in OP compounds cyclosarin, DCP, GV, sarin, soman, VG, VM, and VX, which showed higher absorption wavelength values compared to water ( $\vec{\rho} = 1.85D$ ). It is important to notice that DFP was the only OP that showed an inversion of the behavior, and in water solvent, it showed the highest absorption wavelength values compared to DMSO.

The emission wavelength value was observed in three OPs, DCP, GV, and VG (Table 5). The compounds showed four O atoms bonded with the P atom, and this feature was favorable for charge delocalization and promotion of the fluorescence emission. The other OP compounds dissipated the energy without fluorescence emission. The wavelength in the tested solvents was constant showing less variance. DCP emitted fluorescence at 734 nm, which corresponds to red color emission; GV emitted fluorescence at 420 nm, which corresponds to violet color emission; and VG emitted fluorescence at 570 nm, which corresponds to green color emission.

The main transitions in the absorption process in apolar solvents (hexane, toluene, and chloroform) were from HOMO-1 to LUMO, HOMO-1 to LUMO+1, and HOMO to LUMO. On the other hand, in polar solvents (water and DMSO), only the transition HOMO-LUMO was observed for the absorption process. This effect was observed for all OPs, and the HOMO orbitals involved in the

TABLE 3: Structure of reaction products between dipyrinone oxime and organophosphate compounds according to Scheme 2.

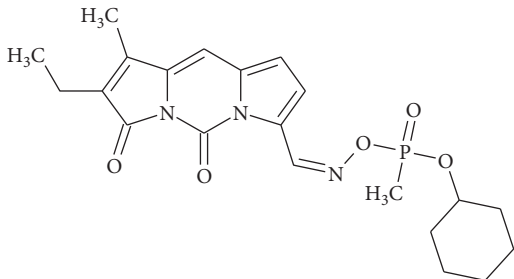
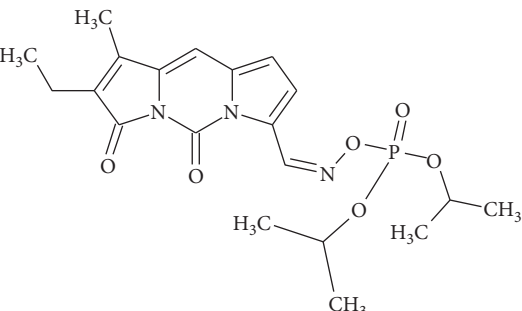
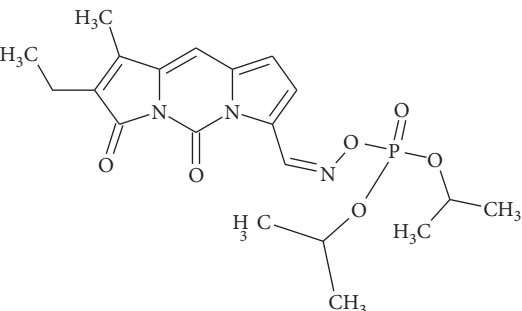
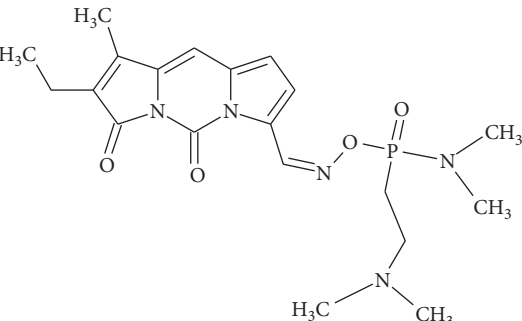
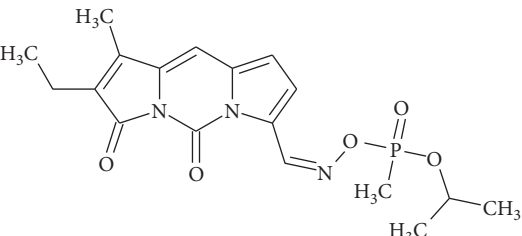
Reaction	Oxime/OP complex
I	
II	
III	
IV	
V	

TABLE 3: Continued.

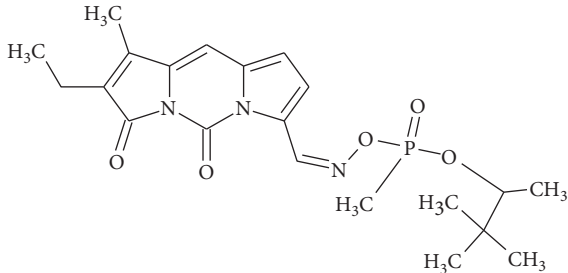
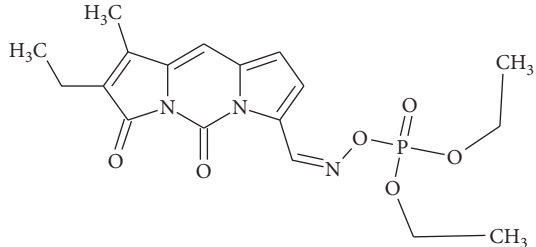
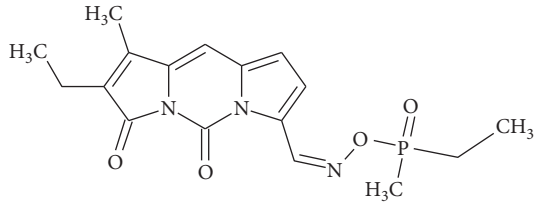
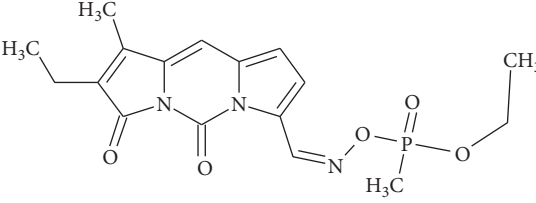
Reaction	Oxime/OP complex
VI	
VII	
VIII	
IX	

TABLE 4: Energy and absorption wavelength of oxime/organophosphate complexes for the eight studied solvents.

		Cyclosarin	DCP*	DFP*	GV*	Sarin	Soman	VG*	VM*	VX*
Hexane	E (eV)	3.78	3.75	3.80	3.76	3.80	3.82	3.78	3.79	3.78
	$\lambda$ (nm)	328	330.8	325.9	329.4	326.2	324.5	327.7	326.4	327.9
Toluene	E (eV)	3.77	3.74	3.79	3.76	3.79	3.81	3.78	3.78	3.78
	$\lambda$ (nm)	328.4	331.2	327.2	329.3	326.8	325.2	327.9	327.4	327.8
Chloroform	E (eV)	3.78	3.76	3.79	3.80	3.78	3.80	3.77	3.79	3.79
	$\lambda$ (nm)	327.9	329.9	326.4	326.2	327.5	326.2	328.3	327	327.3
DCM**	E (eV)	3.78	3.76	3.79	3.79	3.77	3.79	3.78	3.78	3.78
	$\lambda$ (nm)	328	329.6	326.4	326.5	328.2	327.1	328	328	327.8
Methanol	E (eV)	3.78	3.76	3.79	3.80	3.77	3.78	3.78	3.77	3.78
	$\lambda$ (nm)	328	329.1	327.1	325.7	328.7	327.8	327.9	328.4	327.8
Acetonitrile	E (eV)	3.78	3.76	3.79	3.80	3.77	3.78	3.78	3.77	3.78
	$\lambda$ (nm)	328.1	329.2	327.4	325.8	328.8	327.9	328	328.6	327.9
Water	E (eV)	3.78	3.76	3.78	3.80	3.76	3.78	3.78	3.77	3.78
	$\lambda$ (nm)	328.2	329.2	328	325.7	329	328.1	328.1	328.7	328
DMSO**	E (eV)	3.76	3.76	3.79	3.79	3.76	3.77	3.60	3.76	3.80
	$\lambda$ (nm)	328.9	330.1	326.8	326.4	329.6	328.7	328.9	329.4	328.7

\*DCP (diethyl chlorophosphate), DFP (diisopropylfluorophosphate), GV (2-(dimethylamino)ethyl N,N-dimethylphosphoramidofluoridate), VM (O-ethyl-S-[2-(diethylamino)ethyl]methylphosphonothioate), VX (O-ethyl-S-[2(diisopropylamino)ethyl] methylphosphonothioate), and VG (O,O-diethyl-S-[2-(diethylamino)ethyl] phosphorothioate). \*\*Dichloromethane solvent (DCM); dimethyl sulfoxide (DMSO).



TABLE 5: Energy and emission wavelengths of the oxime/organophosphate complex in eight solvents.

OP*		Hexane	Toluene	Chloroform	DCM	Methanol	Acetonitrile	Water	DMSO
DCP	$\lambda$ (nm)	746.7	754.0	742.3	735.3	721.4	722.2	720.2	734.2
	E (eV)	1.66	1.64	1.67	1.68	1.72	1.71	1.72	1.69
GV	$\lambda$ (nm)	423.6	434.5	426.5	422.4	411.6	413.2	411.5	426.2
	E (eV)	2.92	2.85	2.91	2.93	3.01	3.00	3.01	2.91
VG	$\lambda$ (nm)	577.7	582.4	574.7	570.8	562.3	563.3	561.9	572.0
	E (eV)	2.14	2.13	2.15	2.17	2.20	2.20	2.21	2.16

\*DCP (diethyl chlorophosphate), GV (2-(dimethylamino)ethyl N,N-dimethylphosphoramidofluoridate), and VG (O,O-diethyl-S-[2-(diethylamino)ethyl] phosphorothioate). \*\*Dichloromethane solvent (DCM); dimethyl sulfoxide (DMSO).

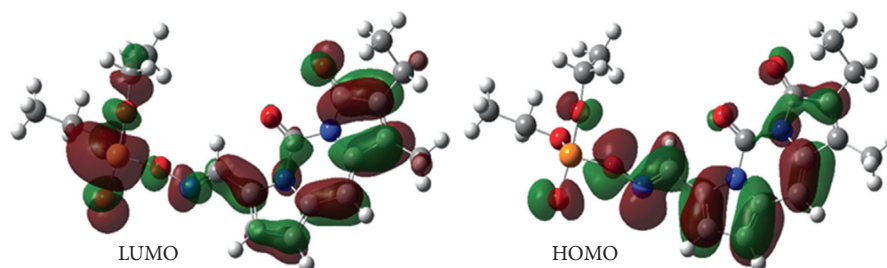


FIGURE 6: Representation of HOMO-LUMO orbitals in the dipyrinone oxime/diethyl chlorophosphate complex.

excitation were localized just in the **1** structure, while the LUMO orbitals are delocalized in **1** as well as in other organophosphorus compounds. The angles observed on the response surface can help in the delocalized orbitals between the organophosphorus and **1** as observed in Figure 6. This feature demonstrates that the conformational structure generated on the response surface was important for orbital delocalizations as well as for the emission process.

#### 4. Conclusion

The DFT and TD-DFT were satisfactory for this study, and the hybrid functional family showed the lowest error when compared with other families. The B3LYP functional exhibited the error inside its family (7.1), being the functional selected for the optimization step as well as absorption and emission property calculations. The surface response analysis showed the energy minimum when angle  $\alpha_1$  was  $25^\circ$  and  $\alpha_2$  was  $0^\circ$ . The solvent analysis showed less variation in the absorption values. The dipolar moment and dielectric constant showed influence on the absorption properties. The reaction between **1** and the OP compounds showed to be kinetically favorable for all compounds, Sarin and cyclosarin are more reactive. The OPs with a sulfur leaving group demonstrated to be more thermodynamically favorable (VX, VG, and VM). The VX reaction showed  $-73$  kcal/mol for  $\Delta G$  and  $-98$  kcal/mol for  $\Delta H$ . The TDA was significant because this methodology describes the solvent effects better [28–30]. Only three compounds showed emission values (DCP, VG, and GV). The emission was influenced by HOMO – 1-LUMO, HOMO-LUMO, and HOMO-LUMO + 1 transitions. The conformational structure generated on the response surface was important for orbital delocalization between oxime and organophosphates. The understanding

of the nature of the emission and the solvent influence was important for this study because it allows proposing new ways for compound structural modifications in order to build more efficient fluorescent probes.

#### Data Availability

Values for angles and energies of ground states (GS) and excited states (ES) in gas as well as in water solution are included within the supporting information. The other data used to support the finding of this study are included in the article, and if further data related to analysis are required, the corresponding author can provide upon request.

#### Conflicts of Interest

The authors declare that they have no conflicts of interest.

#### Acknowledgments

The authors thank the Brazilian agencies FAPEMIG, CAPES, and CNPq for the financial support of this research and UFPA for infrastructure and encouragement in this work. This work was also supported by Excellence project FIM and by the University of Hradec Kralove (Faculty of Science, VT2019-2021).

#### Supplementary Materials

S1. Surface response. Table S1: values for angles, energies of ground state (GS) and excited state (ES), and wavelength calculated for combination of angles employed for building surface response. Table S2: values for angles, energies of ground state (GS) and excited state (ES), and wavelength calculated for combination of angles employed for building

surface response in water solvent. Table S3: values for geometric properties from organophosphorus compounds and the complex with oxime (distance). (*Supplementary Materials*)

## References

- [1] W. E. A. de Lima, A. F. Pereira, A. A. de Castro, E. F. F. da Cunha, and T. C. Ramalho, "Flexibility in the molecular design of acetylcholinesterase reactivators: probing representative conformations by chemometric techniques and docking/QM calculations," *Letters in Drug Design & Discovery*, vol. 13, no. 5, pp. 360–371, 2016.
- [2] H. Zhang, X. Hua, X. Tuo, C. Chen, and X. Wang, "Polystyrene microsphere-based lanthanide luminescent chemosensor for detection of organophosphate pesticides," *Journal of Rare Earths*, vol. 30, no. 12, pp. 1203–1207, 2012.
- [3] H. A. Azab, A. Duerkop, Z. M. Anwar, B. H. M. Hussein, M. A. Rizk, and T. Amin, "Luminescence recognition of different organophosphorus pesticides by the luminescent Eu(III)-pyridine-2,6-dicarboxylic acid probe," *Analytica Chimica Acta*, vol. 759, pp. 81–91, 2013.
- [4] V. M. R. d. Santos, C. L. Donnici, J. B. N. DaCosta, and J. M. R. Caixeiro, "Compostos organofosforados pentavalentes: histórico, métodos sintéticos de preparação e aplicações como inseticidas e agentes antitumorais," *Química Nova*, vol. 30, no. 1, pp. 159–170, 2007.
- [5] G. Yue, S. Su, N. Li et al., "Gold nanoparticles as sensors in the colorimetric and fluorescence detection of chemical warfare agents," *Coordination Chemistry Reviews*, vol. 311, pp. 75–84, 2016.
- [6] N. Singh, Y. Karpichev, A. K. Tiwari, K. Kuca, and K. K. Ghosh, "Oxime functionality in surfactant self-assembly: an overview on combating toxicity of organophosphates," *Journal of Molecular Liquids*, vol. 208, pp. 237–252, 2015.
- [7] M. Singh, M. Kaur, H. Kukreja, R. Chugh, O. Silakari, and D. Singh, "Acetylcholinesterase inhibitors as Alzheimer therapy: from nerve toxins to neuroprotection," *European Journal of Medicinal Chemistry*, vol. 70, pp. 165–188, 2013.
- [8] C. Scheffel, H. Thiermann, and F. Worek, "Effect of reversible ligands on oxime-induced reactivation of sarin- and cyclo-sarin-inhibited human acetylcholinesterase," *Toxicology Letters*, vol. 232, no. 3, pp. 557–565, 2015.
- [9] Y. Liu, H. Yu, L. Zhao, and H. Zhang, "Radiolabeled Zn-DPA as a potential infection imaging agent," *Nuclear Medicine and Biology*, vol. 39, no. 5, pp. 126–134, 2012.
- [10] M. Winter, T. Wille, K. Musilek, K. Kuca, H. Thiermann, and F. Worek, "Investigation of the reactivation kinetics of a large series of bispyridinium oximes with organophosphate-inhibited human acetylcholinesterase," *Toxicology Letters*, vol. 244, pp. 136–142, 2016.
- [11] A. Kulakova, S. Lushchekina, B. Grigorenko, and A. Nemukhin, "Modeling reactivation of the phosphorylated human butyrylcholinesterase by QM (DFTB)/MM calculations," *Journal of Theoretical and Computational Chemistry*, vol. 14, no. 7, Article ID 1550051, 2015.
- [12] D. M. Maxwell, K. M. Brecht, and R. E. Sweeney, "A common mechanism for resistance to oxime reactivation of acetylcholinesterase inhibited by organophosphorus compounds," *Chemico-Biological Interactions*, vol. 203, no. 1, pp. 72–76, 2013.
- [13] J. Bajgar, K. Kuca, D. Jun, L. Bartosova, and J. Fusek, "Cholinesterase reactivators: the fate and effects in the organism poisoned with organophosphates/nerve agents," *Current Drug Metabolism*, vol. 8, no. 8, pp. 803–809, 2007.
- [14] Z. Radić, J. Kalisiak, V. V. Fokin, K. B. Sharpless, and P. Taylor, "Interaction kinetics of oximes with native, phosphorylated and aged human acetylcholinesterase," *Chemico-Biological Interactions*, vol. 187, no. 1–3, pp. 163–166, 2010.
- [15] N. Chadha, M. S. Bahia, M. Kaur, and O. Silakari, "Thiazolidine-2,4-dione derivatives: programmed chemical weapons for key protein targets of various pathological conditions," *Bioorganic & Medicinal Chemistry*, vol. 23, no. 13, pp. 2953–2974, 2015.
- [16] A. M. Romero, "Commercializing chemical warfare: citrus, cyanide, and an endless war," *Agriculture and Human Values*, vol. 33, no. 1, pp. 3–26, 2016.
- [17] I. Walton, M. Davis, L. Munro et al., "A fluorescent dipyrinone oxime for the detection of pesticides and other organophosphates," *Organic Letters*, vol. 14, no. 11, pp. 2686–2689, 2012.
- [18] K. L. Nash, C. Lavallette, M. Borkowski, R. T. Paine, and X. Gan, "Features of the thermodynamics of two-phase distribution reactions of americium(III) and europium(III) nitrates into solutions of 2,6-Bis[(bis(2-ethylhexyl)phosphino)methyl]pyridineN,P,P'-Trioxide," *Inorganic Chemistry*, vol. 41, no. 22, pp. 5849–5858, 2002.
- [19] H. Wang, G. Zhou, C. Mao, and X. Chen, "A fluorescent sensor bearing nitroolefin moiety for the detection of thiols and its biological imaging," *Dyes and Pigments*, vol. 96, no. 1, pp. 232–236, 2013.
- [20] M. E. Casida and M. Huix-Rotllant, "Progress in time-dependent density-functional theory," *Annual Review of Physical Chemistry*, vol. 63, no. 1, pp. 287–323, 2012.
- [21] E. P. da Rocha, A. A. Castro, T. C. Ramalho, and E. F. F. da Cunha, "Insights into the value of statistical models and relativistic effects for the investigation of halogenated derivatives of fluorescent probes," *Theoretical Chemistry Accounts*, vol. 135, no. 5, p. 135, 2016.
- [22] D. Jacquemin, E. A. Perpète, G. E. Scuseria, I. Ciofini, and C. Adamo, "TD-DFT performance for the visible absorption spectra of organic dyes: conventional versus long-range hybrids," *Journal of Chemical Theory and Computation*, vol. 4, no. 1, pp. 123–135, 2008.
- [23] K. Guzow, M. Milewska, C. Czaplowski, and W. Wiczak, "A DFT/TD DFT study of the structure and spectroscopic properties of 5-methyl-2-(8-quinolinyl)benzoxazole and its complexes with Zn(II) ion," *Spectrochimica Acta Part A: Molecular and Biomolecular Spectroscopy*, vol. 75, no. 2, pp. 773–781, 2010.
- [24] D. Yang, F. Zhao, R. Zheng, Y. Wang, and J. Lv, "A detailed theoretical investigation on the excited-state intramolecular proton-transfer mechanism of 3-BTHPB chemosensor," *Theoretical Chemistry Accounts*, vol. 134, no. 5, p. 62, 2015.
- [25] Y. Shao, L. F. Molnar, Y. Jung et al., "Advances in methods and algorithms in a modern quantum chemistry program package," *Physical Chemistry Chemical Physics*, vol. 8, no. 27, pp. 3172–3191, 2006.
- [26] H. Roohi, F. Hejazi, N. Mohtamedifar, and M. Jahantab, "Excited state intramolecular proton transfer (ESIPT) in 2-(2'-hydroxyphenyl)benzoxazole and its naphthalene-fused analogs: a TD-DFT quantum chemical study," *Spectrochimica Acta Part A: Molecular and Biomolecular Spectroscopy*, vol. 118, pp. 228–238, 2014.
- [27] Q. Sun, S. Mosquera-Vazquez, Y. Suffren et al., "On the role of ligand-field states for the photophysical properties of ruthenium(II) polypyridyl complexes," *Coordination Chemistry Reviews*, vol. 282–283, no. 1, pp. 87–99, 2015.

- [28] A. Chantzis, A. D. Laurent, C. Adamo, and D. Jacquemin, "Is the Tamm-Dancoff approximation reliable for the calculation of absorption and fluorescence band shapes?" *Journal of Chemical Theory and Computation*, vol. 9, no. 10, pp. 4517–4525, 2013.
- [29] M. E. Casida, F. Gutierrez, J. Guan, F.-X. Gadea, D. Salahub, and J.-P. Daudey, "Charge-transfer correction for improved time-dependent local density approximation excited-state potential energy curves: analysis within the two-level model with illustration for H<sub>2</sub> and LiH," *The Journal of Chemical Physics*, vol. 113, no. 17, pp. 7062–7071, 2000.
- [30] S. Grimme and F. Neese, "Double-hybrid density functional theory for excited electronic states of molecules," *The Journal of Chemical Physics*, vol. 127, no. 15, p. 154116, 2007.
- [31] F. Neese, "The ORCA program system," *WIREs Computational Molecular Science*, vol. 2, no. 1, pp. 73–78, 2012.
- [32] F. S. Miranda, C. M. Ronconi, M. O. B. Sousa, G. Q. Silveira, and M. D. Vargas, "6-Aminocoumarin-naphthoquinone conjugates: design, synthesis, photophysical and electrochemical properties and DFT calculations," *Journal of the Brazilian Chemical Society*, vol. 25, no. 1, pp. 133–142, 2014.
- [33] T. Yanai, D. P. Tew, and N. C. Handy, "A new hybrid exchange-correlation functional using the Coulomb-attenuating method (CAM-B3LYP)," *Chemical Physics Letters*, vol. 393, no. 1–3, pp. 51–57, 2004.
- [34] R. Kobayashi and R. D. Amos, "The application of CAM-B3LYP to the charge-transfer band problem of the zincbacteriochlorin-bacteriochlorin complex," *Chemical Physics Letters*, vol. 420, no. 1–3, pp. 106–109, 2006.
- [35] J. C. d. Santos, J. A. A. de França, L. E. do Nascimento Aquino et al., "Theoretical calculation and structural studies for a new nitrogen derivative from nor-lapachol," *Journal of Molecular Structure*, vol. 1060, no. 1, pp. 233–238, 2014.
- [36] A. D. Laurent and D. Jacquemin, "TD-DFT benchmarks: a review," *International Journal of Quantum Chemistry*, vol. 113, no. 17, pp. 2019–2039, 2013.
- [37] S. Chibani, D. Jacquemin, and A. D. Laurent, "Modelling solvent effects on the absorption and emission spectra of constrained cyanines with both implicit and explicit QM/EFP models," *Computational and Theoretical Chemistry*, vol. 1040–1041, pp. 321–327, 2014.
- [38] A. D. Laurent, Y. Houari, P. H. P. R. Carvalho, B. a. D. Neto, and D. Jacquemin, "ESIPT or not ESIPT? Revisiting recent results on 2,1,3-benzothiadiazole under the TD-DFT light," *RSC Advances*, vol. 4, no. 27, pp. 14189–14192, 2014.
- [39] E. A. Songa and J. O. Okonkwo, "Recent approaches to improving selectivity and sensitivity of enzyme-based biosensors for organophosphorus pesticides: a review," *Talanta*, vol. 155, pp. 289–304, 2016.
- [40] J. Chang, H. Li, T. Hou, and F. Li, "Paper-based fluorescent sensor for rapid naked-eye detection of acetylcholinesterase activity and organophosphorus pesticides with high sensitivity and selectivity," *Biosensors and Bioelectronics*, vol. 86, pp. 971–977, 2016.
- [41] M. A. Shameem and A. Orthaber, "Organophosphorus compounds in organic electronics," *Chemistry-A European Journal*, vol. 22, no. 31, pp. 10718–10735, 2016.
- [42] T. M. de Assis, G. C. Gajo, L. C. de Assis et al., "QSAR models guided by molecular dynamics applied to human glucokinase activators," *Chemical Biology & Drug Design*, vol. 87, no. 3, pp. 455–466, 2016.
- [43] M. A. Gonçalves, F. C. Peixoto, E. F. F. da Cunha, and T. C. Ramalho, "Dynamics, NMR parameters and hyperfine coupling constants of the Fe<sub>3</sub>O<sub>4</sub>(100)-water interface: implications for MRI probes," *Chemical Physics Letters*, vol. 609, pp. 88–92, 2014.
- [44] M. A. Gonçalves, E. F. F. da Cunha, F. C. Peixoto, and T. C. Ramalho, "Probing thermal and solvent effects on hyperfine interactions and spin relaxation rate of δ-FeOOH(100) and [MnH<sub>3</sub>buea(OH)]<sup>2-</sup>: toward new MRI probes," *Computational and Theoretical Chemistry*, vol. 1069, pp. 96–104, 2015.
- [45] D. T. Mancini, K. Sen, M. Barbatti, W. Thiel, and T. C. Ramalho, "Excited-state proton transfer can tune the color of protein fluorescent markers," *ChemPhysChem*, vol. 16, no. 16, pp. 3444–3449, 2015.
- [46] D. T. Mancini, E. F. Souza, M. S. Caetano, and T. C. Ramalho, "99Tc NMR as a promising technique for structural investigation of biomolecules: theoretical studies on the solvent and thermal effects of phenylbenzothiazole complex," *Magnetic Resonance in Chemistry*, vol. 52, no. 4, pp. 129–137, 2014.
- [47] E. P. Rocha and T. C. Ramalho, "Probing the ESIPT process in 2-amino-1, 4-naphthoquinone: thermodynamics properties, solvent effect and chemometric analysis," *Theoretical Chemistry Accounts*, vol. 135, no. 2, p. 39, 2016.
- [48] S. L. C. Ferreira, R. E. Bruns, E. G. P. da Silva et al., "Statistical designs and response surface techniques for the optimization of chromatographic systems," *Journal of Chromatography A*, vol. 1158, no. 1–2, pp. 2–14, 2007.
- [49] T. Lundstedt, E. Seifert, L. Abramo et al., "Experimental design and optimization," *Chemometrics and Intelligent Laboratory Systems*, vol. 42, no. 1–2, pp. 3–40, 1998.
- [50] K. Chen, W. Yan, X. Zhang, Y. Kuang, X. Tang, and X. Han, "Optimization of process variables in the synthesis of isoamyl isovalerate using sulfonated organic heteropolyacid salts as catalysts," *Journal of the Brazilian Chemical Society*, vol. 26, no. 3, pp. 600–608, 2015.
- [51] N. Aslan and Y. Cebeci, "Application of Box-Behnken design and response surface methodology for modeling of some Turkish coals," *Fuel*, vol. 86, no. 1–2, pp. 90–97, 2007.
- [52] M. A. Bezerra, R. E. Santelli, E. P. Oliveira, L. S. Villar, and L. A. Escalera, "Response surface methodology (RSM) as a tool for optimization in analytical chemistry," *Talanta*, vol. 76, no. 5, pp. 965–977, 2008.
- [53] S. Krol, "Challenges in drug delivery to the brain: nature is against us," *Journal of Controlled Release*, vol. 164, no. 2, pp. 145–155, 2012.
- [54] T. R. Papo and D. Jaganyi, "Kinetic and mechanistic investigation into the influence of substituents on the substitution reactions of Pt(II) NCN-donor complexes," *Transition Metal Chemistry*, vol. 40, no. 1, pp. 53–60, 2015.
- [55] T. L. C. Martins, T. C. Ramalho, J. D. Figueroa-Villar, A. F. C. Flores, and C. U. M. P. Pereira, "Theoretical and experimental <sup>13</sup>C and <sup>15</sup>N NMR investigation of guanlylhydrazones in solution," *Magnetic Resonance in Chemistry*, vol. 41, no. 12, pp. 983–988, 2003.
- [56] J. B. d. R. Lino and T. C. Ramalho, "Exploring through-space spin-spin couplings for quantum information processing: facing the challenge of coherence time and control quantum states," *The Journal of Physical Chemistry A*, vol. 123, no. 7, pp. 1372–1379, 2019.
- [57] T. C. Ramalho, M. V. J. Rocha, E. F. F. da Cunha, L. C. A. Oliveira, and K. T. G. Carvalho, "Understanding the molecular behavior of organotin compounds to design their effective use as agrochemicals: exploration via quantum chemistry and experiments," *Journal of Biomolecular Structure and Dynamics*, vol. 28, no. 2, pp. 227–238, 2010.